J. Fluid Mech. (1996), vol. 320, pp. 417–443

The second-order wave force on a vertical cylinder

By J. N. NEWMAN

Department of Ocean Engineering, Massachusetts Institute of Technology,
Cambridge, MA 02139, USA
email:jnn@mit.edu

(Received 27 November 1995 and in revised form 1 April 1996)

The second-order wave force is analysed for diffraction of monochromatic water waves by a vertical cylinder. The force is evaluated directly from pressure integration over the cylinder, and the second-order potential is derived by Weber transformation of the corresponding forcing function on the free surface. This forcing function is reduced to a form which involves a simple factor inversely proportional to the radial coordinate plus an oscillatory function which decays more rapidly in the far field. This feature alleviates the slow rate of convergence involved in capturing the far-field effect. Benchmark computations are obtained and compared with other works. Asymptotic approximations are derived for long and short wavelengths. The analysis and results are primarily for the case of infinite fluid depth, but the finite-depth case is also considered to facilitate comparison with other computations and to illustrate the importance of finite-depth effects in the long-wavelength asymptotic regime.

1. Introduction

Many theoretical studies have been made concerning the diffraction of water waves by a circular cylinder with vertical axis which extends throughout a fluid of infinite or finite depth. This problem has great practical significance, since many offshore platforms and other structures are supported by vertical columns of circular form which are subject to wave loads. Potential theory is applicable, provided the wave height does not exceed a magnitude comparable to the diameter of the columns. If the wave slope is sufficiently small to justify linearization, the velocity potential can be derived by separation of variables, in the manner outlined by Havelock (1929). The solution is an infinite series of eigenfunctions which correspond to the terms of a Fourier series in the angular coordinate θ. The radial functions are appropriate combinations of Bessel and Hankel functions (cf. equation (2.2) below). The resulting first-order hydrodynamic force, proportional to the wave amplitude A, was first derived for infinite depth by Havelock (1940), and extended to the more general case of a fluid of finite depth by MacCamy & Fuchs (1954) (cf. Mei 1983, equation 5.8). Various extensions of this simple problem have been considered including an elegant theory for arrays of circular cylinders (Linton & Evans 1990), and numerical solutions for more general bodies.

Second-order wave forces proportional to A^2 have particular importance in certain applications. In regular waves the second-order force includes a mean 'drift

force' which is constant in time, and a second-harmonic component. In a spectrum these are generalized to include low 'difference-frequency' and high 'sum-frequency' components, respectively. These have special significance in regard to tension-leg platforms, and other types of vessels which are designed to have small response at the frequencies of first-order wave loads but which suffer from highly tuned resonant motions at frequencies below or above the first-order spectral range. These problems are surveyed by Molin (1994).

In regular waves the drift force can be evaluated completely from the first-order velocity potential in a relatively simple manner, as first shown by Havelock (1940). The second-harmonic component is more difficult to analyse since it depends in part on the second-order component of the velocity potential, which is forced by quadratic interactions of the first-order solution over the domain of the free surface.

This paper is concerned only with the second-harmonic force which acts on a vertical cylinder in regular waves. The theoretical formulation of this problem was first developed by Molin (1979), in the manner which is generally accepted to be complete and correct. Molin provided an appropriate modification of the Sommerfeld radiation condition which is applicable to the second-order potential and, following the analogous two-dimensional work of Faltinsen & Løken (1978), Molin also showed that the second-order force can be derived in an 'indirect' manner using Green's theorem. This circumvents the need to solve for the second-order potential, although the numerical effort is not reduced significantly. Lighthill (1979) publicized this indirect approach, and derived the necessary 'assisting potential' for a vertical cylinder of infinite depth.

The problem of a vertical cylinder in infinite depth was studied by Hunt & Baddour (1981) using the direct approach, and subsequently extended to finite depth by Hunt & Williams (1982). Their works appear to involve a different interpretation of the far-field condition, and Molin's results were criticized. Nevertheless, the final formulae of Hunt and co-workers are in fact correct for the second-order force, although their numerical results are not reliable. More complete results have been presented by Eatock Taylor & Hung (1987), who followed the indirect approach of Lighthill (1979) and presented extensive computations including both cases where the fluid depth is infinite or finite. Comparisons were made with the computations of Hunt and co-workers and significant differences were noted in some cases. Further computations were presented for truncated cylinders of finite draught by Kim & Yue (1989), and for the special case of a bottom-mounted cylinder in a fluid of finite depth results were given based on both the direct and indirect approach. Second-order panel methods have been developed subsequently which are applicable for more general bodies.

The present work is motivated in part by the need for accurate numerical results suitable for use as benchmarks in testing panel programs, and by the inconsistencies in some of the earlier papers listed above. The direct approach is used, a Weber transform is employed to solve for the second-order potential in the same manner as first applied to this problem by Hunt & Baddour (1981), and the resulting pressure is integrated over the body surface. It is interesting to note that the indirect approach of Eatock Taylor & Hung (1987) and the present direct solution lead to identical analytical expressions for the second-order force. One feature of the direct solution based on Weber transformation is that the far-field asymptotic form of the second-order potential is easily derived in terms of the 'locked' and 'free' components first elucidated by Molin (1979).

To simplify the analysis we restrict our attention to the first Fourier harmonic of

the second-order potential, with respect to the angular coordinate θ, since this is the only component which affects the integrated force. A more complete solution for the second-order potential is derived by Chau & Eatock Taylor (1992), using a special Green function which satisfies both the first-order free-surface condition and the homogeneous Neumann condition on the cylinder. That procedure and the use of Weber transforms are fundamentally equivalent, but the latter approach appears to be somewhat simpler and more direct.

An important detail from the computational standpoint is that we reduce the expression for the forcing function of the second-order potential on the free surface to a form which is simpler to apply. This feature, and the use of integration in the complex plane, alleviate the most difficult computational aspect of the second-order analysis, involving slowly convergent integration over the free surface. The latter problem is elaborated by Kim & Yue (1989) and by Chau & Eatock Taylor (1992). The present approach permits us to compute the second-harmonic force with high numerical accuracy, for a broad range of wavenumbers.

To complete the description of the second-order force we also derive asymptotic approximations in the complementary regimes where the wavelength is either long ($Ka \ll 1$) or short ($Ka \gg 1$) compared to the cylinder radius.

The long-wavelength regime is of practical importance in regard to many offshore platforms where the surface-piercing elements are cylindrical columns with diameters of 10–20 m. In severe sea states where the characteristic wavelengths are 200–400 m it follows that $Ka < \pi/10$. This consideration has motivated long-wavelength approximations for the first- and second-order forces which are derived by Lighthill (1979). At first order a local analysis is justified and the resulting limit of the first-order force is consistent with the inertial term of Morison's formula, i.e. a force acting on the cylinder proportional to the product of the local horizontal acceleration of the incident-wave field and the virtual mass. A more complete solution is required to account for the free-surface forcing effect on the second-order potential, which acts over relatively large horizontal scales, as emphasized by Newman (1990). The long-wavelength approximation of the second-order force derived by Lighthill (1979) is incomplete in this respect, and a more consistent approximation is derived here, but little practical improvement results from this refinement.

The long-wavelength regime is important not only for first- and second-order forces but at higher order in connection with the problem of 'ringing', which has been observed on some types of offshore platforms in extreme wave conditions. A conflict in the study of the third-order third-harmonic force has emerged from two somewhat different theories developed by Faltinsen, Newman & Vinje (1995) and by Malenica & Molin (1995). In Faltinsen *et al.* the fundamental assumptions are that $Ka \ll 1$ and $A/a = O(1)$, whereas in Malenica & Molin $Ka = O(1)$ and $A \ll a$. Another difference is that Faltinsen *et al.* assume the fluid depth to be infinite, whereas Malenica & Molin consider the depth to be finite. In seeking an explanation for the limited agreement between these complementary theories Malenica & Molin note that the long-wavelength approximation has a rather restricted domain of applicability also in the second-order theory. Thus a more complete study of the second-order problem is warranted, including a consideration of the different long-wavelength results which correspond to the cases of finite and infinite depth.

The short-wavelength regime is interesting insofar as the second-order force is oscillatory, in phase with the reflected waves along the ray opposite to the incident-wave direction, and the modulus of the force increases in proportion to the frequency

for fixed incident-wave amplitude. This (horizontal) force is due primarily to the pressure field at large depths relative to the wavelength, as in the analogous case of the vertical force on a deep truncated cylinder (Newman 1990).

Our analysis is focused on the second-harmonic force F_2 which acts on the cylinder. This component of the total second-order force can be expressed in the form

$$F_2 = \mathrm{Re}\left\{\left(F_q + F_p\right) \mathrm{e}^{2\mathrm{i}\omega t}\right\}, \tag{1.1}$$

where ω is the frequency of the first-order motion, F_q is the component due to quadratic contributions from the first-order potential, and F_p is due to the second-order potential itself. These are considered separately in the following sections.

The case of an infinite fluid depth is considered first, to simplify the analysis. In §2 the first-order potential is reviewed, and applied to the force F_q. The free-surface forcing function for the second-order potential is derived in §3, the solution is obtained in §4, and the resulting force F_p is evaluated in §5. Long- and short-wavelength approximations for F_q and F_p are derived in §6 and §7. The corresponding analysis for a fluid of finite depth is summarized in §§8–10. The results are discussed in the concluding §11.

It is convenient to non-dimensionalize the force F_2, and each of its components, dividing by the product $\rho g A^2 a$ where ρ is the fluid density, g the acceleration due to gravity, A the incident-wave amplitude, and a the cylinder radius. Denoting the non-dimensional force with an overbar,

$$F_2 = \rho g A^2 a \bar{F}_2 = \rho g A^2 a\, \mathrm{Re}\left\{\left(\bar{F}_q + \bar{F}_p\right) \mathrm{e}^{2\mathrm{i}\omega t}\right\}. \tag{1.2}$$

In §§8–10, where the fluid depth is finite, the additional decomposition

$$\bar{F}_p = \bar{F}_I + \bar{F}_B \tag{1.3}$$

is made, where $\bar{F}_I$ is the contribution associated with the second-order component of the incident-wave potential, and with the scattering of this potential by the cylinder, and $\bar{F}_B$ is the contribution from the remaining second-order potential.

2. Force due to the first-order potential

We consider the scattering of plane progressive waves by a vertical circular cylinder of radius a, which extends throughout the fluid of infinite depth. The first-order diffraction potential can be expressed in the form

$$\Phi_1 = \mathrm{Re}\left\{\phi_1 \mathrm{e}^{\mathrm{i}\omega t}\right\} \tag{2.1}$$

where ω is the radian frequency, t denotes time, and

$$\phi_1 = (\mathrm{i}gA/\omega)\, \mathrm{e}^{Kz} \sum_{m=0}^{\infty} \epsilon_m \mathrm{i}^{-m} \cos m\theta\, R_m(Kr). \tag{2.2}$$

Here $A\cos\omega t$ is the incident-wave elevation at the cylinder axis, g is the gravitational acceleration, and $K = \omega^2/g$ is the wavenumber. The cylindrical coordinates (r, θ, z) are defined such that $z = 0$ is the plane of the undisturbed free surface, $z < 0$ is the fluid domain, and the direction of wave propagation is $\theta = 0$. The symbol ϵ_m denotes the Jacobi factor: $\epsilon_0 = 1$ and $\epsilon_m = 2$ for $m \geqslant 1$. The radial functions $R_m(Kr)$ are defined by

$$R_m(Kr) = J_m(Kr) - c_m H_m(Kr), \tag{2.3}$$

where $H_m = J_m - iY_m$ is the Hankel function of the second kind, and for convenience the usual superscript (2) is omitted. The coefficients c_m are evaluated so that (2.2) satisfies the boundary condition of zero normal velocity on the cylinder, hence

$$c_m(Ka) = J'_m(Ka)/H'_m(Ka). \tag{2.4}$$

The total integrated force acting on the cylinder in the direction $\theta = 0$, due to the fluid pressure p, is

$$F = \rho a \int_0^{2\pi} \cos\theta \, d\theta \int_{-\infty}^{\zeta} \left(\Phi_t + \tfrac{1}{2}\nabla\Phi\cdot\nabla\Phi + gz\right)_{r=a} dz. \tag{2.5}$$

Here the Bernoulli equation has been used to evaluate the pressure, and $z = \zeta$ is the elevation of the free surface. The linear force is derived in a straightforward manner by substituting (2.1) for the term Φ_t, and integrating below the mean free surface $z = 0$.

In the analysis to follow we consider only the second-harmonic components of second-order quantities, for which the general relation

$$\mathrm{Re}\left\{U e^{i\omega t}\right\} \mathrm{Re}\left\{V e^{i\omega t}\right\} = \tfrac{1}{2}\mathrm{Re}\left\{UV e^{2i\omega t} + UV^*\right\} \tag{2.6}$$

may be used. Here an asterisk denotes the complex conjugate, and (U, V) are arbitrary complex coefficients. The last term in (2.6) is omitted hereafter, since it contributes only to the time-average component and not to the second-harmonic.

The first-order potential (2.1) contributes two different components to the second-order force, including the *distributed* force due to the second-order term in the pressure,

$$F_q^{(1)} = \tfrac{1}{4}\rho a \int_0^{2\pi} \cos\theta \, d\theta \int_{-\infty}^{0} (\nabla\phi_1\cdot\nabla\phi_1)\, dz, \tag{2.7}$$

and the *point* force, given by the second-harmonic component of the expression

$$\rho a \int_0^{2\pi} \cos\theta \, d\theta \int_0^{\zeta} (\Phi_t + gz)_{r=a}\, dz = -\tfrac{1}{2}\rho g a \int_0^{2\pi} \cos\theta\, \zeta^2 d\theta. \tag{2.8}$$

Here the relation $\zeta = -(1/g)\Phi_{1t}$ has been used for the first-order free-surface elevation.

For the distributed force (2.7) the vertical integration is elementary, and the azimuthal integral can be evaluated using orthogonality of the Fourier series in the form

$$\int_0^{2\pi} (\nabla\phi_1\cdot\nabla\phi_1)\cos\theta \, d\theta = 4\pi i(gA/\omega)^2 K^2 e^{2Kz} S(Kr), \tag{2.9}$$

where

$$S(Kr) = \sum_{m=0}^{\infty} (-)^m \left(R_m R_{m+1} + R'_m R'_{m+1} + \frac{m(m+1)}{K^2 r^2} R_m R_{m+1}\right). \tag{2.10}$$

On the cylinder $r = a$, $R'_m = 0$ and, from the Wronskian relation for the Bessel functions,

$$R_m = -\frac{2i}{\pi K a H'_m}. \tag{2.11}$$

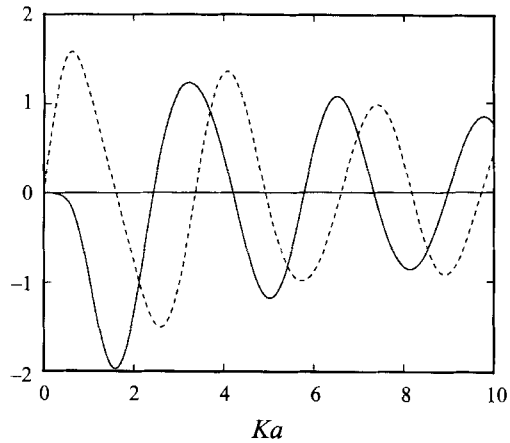

FIGURE 1. Real (solid) and imaginary (dashed) parts of the force $\bar{F}_q$ due to the first-order potential, computed from (2.14).

After substituting these results in (2.7), integrating vertically, and non-dimensionalizing in accordance with (1.2), the distributed force follows in the form

$$\bar{F}_q^{(1)} = -\frac{2\mathrm{i}}{\pi(Ka)^2} \sum_{m=0}^{\infty} (-)^m \left(\frac{1}{H'_m H'_{m+1}} \right) \left(1 + \frac{m(m+1)}{K^2 a^2} \right) . \tag{2.12}$$

A similar analysis for the point force (2.8) gives

$$\bar{F}_q^{(2)} = -\frac{4\mathrm{i}}{\pi(Ka)^2} \sum_{m=0}^{\infty} (-)^m \left(\frac{1}{H'_m H'_{m+1}} \right) . \tag{2.13}$$

Thus the total second-order force due to the first-order potential is

$$\bar{F}_q = -\frac{2\mathrm{i}}{\pi(Ka)^2} \sum_{m=0}^{\infty} (-)^m \left(\frac{1}{H'_m H'_{m+1}} \right) \left(3 + \frac{m(m+1)}{K^2 a^2} \right) . \tag{2.14}$$

Figure 1 shows the results of computations based on direct summation of the series in (2.14), with truncation when the index m exceeds the value $1.5Ka + 8$. The Hankel functions are evaluated from double-precision subroutines based on Chebyshev polynomial approximations. These algorithms are intended to provide at least 8 decimal-place absolute accuracy. The oscillatory behaviour which is evident in figure 1 will be discussed in the context of the short-wavelength asymptotic approximations in §7.

3. The forcing function for the second-order potential

Next we consider the second-order potential ϕ_2 in the perturbation expansion

$$\Phi = \mathrm{Re}\left\{ \phi_1 \mathrm{e}^{\mathrm{i}\omega t} + \phi_2 \mathrm{e}^{2\mathrm{i}\omega t} + \ldots \right\} . \tag{3.1}$$

Like the first-order potential (2.2), ϕ_2 satisfies the homogeneous boundary condition $\phi_{2r} = 0$ on the cylinder, but on the plane $z = 0$ the second-order free-surface condition is applicable. For the present case where the fluid is infinitely deep, and the first-order

solution (2.2) has the same exponential dependence on z as the incident wave, the free-surface condition takes the relatively simple form

$$4K\phi_2 - \phi_{2z} = \frac{\mathrm{i}\omega}{g}\nabla\phi_1 \cdot \nabla\phi_1 . \tag{3.2}$$

The potential ϕ_2 can be expanded in a Fourier series, in the form

$$\phi_2(r,\theta,z) = \sum_{m=0}^{\infty} \phi_2^{(m)}(r,z)\cos m\theta . \tag{3.3}$$

Only the term proportional to $\cos\theta$ contributes to the second-order force (2.5), and from (3.2) the relevant free-surface boundary condition is

$$4K\phi_2^{(1)} - \phi_{2z}^{(1)} = \frac{\mathrm{i}\omega}{\pi g}\int_0^{2\pi} \cos\theta\, \nabla\phi_1 \cdot \nabla\phi_1 \,\mathrm{d}\theta = -4\omega K A^2 S(Kr), \tag{3.4}$$

where $S(Kr)$ is defined by (2.10). This series can be simplified using the relations

$$\mathscr{C}'_m = -\mathscr{C}_{m+1} + \frac{m}{z}\mathscr{C}_m , \quad \mathscr{C}'_{m+1} = \mathscr{C}_m - \frac{m+1}{z}\mathscr{C}_{m+1} , \tag{3.5}$$

where $\mathscr{C}_m$ denotes either the Bessel or Hankel function of argument z. Thus

$$\begin{aligned} S(Kr) = \sum_{m=0}^{\infty}(-)^m \Bigg[& \frac{m}{Kr}J_m^2 + \frac{m+1}{Kr}J_{m+1}^2 \\ & - c_m\left(H_m J_{m+1} - H_{m+1}J_m + \frac{m}{Kr}H_m J_m + \frac{m+1}{Kr}H_{m+1}J_{m+1}\right) \\ & - c_{m+1}\left(J_m H_{m+1} - J_{m+1}H_m + \frac{m}{Kr}J_m H_m + \frac{m+1}{Kr}J_{m+1}H_{m+1}\right) \\ & + c_m c_{m+1}\left(\frac{m}{Kr}H_m^2 + \frac{m+1}{Kr}H_{m+1}^2\right)\Bigg] . \end{aligned} \tag{3.6}$$

The sum of the first two terms in square brackets is zero. (These terms are associated only with the incident-wave potential, for which the right-hand side of (3.2) vanishes.)

After re-grouping the remaining terms in (3.6) and using the Wronskian relation, this equation may be written in the simpler form

$$S(Kr) = \frac{1}{Kr}\left[d_0(Ka) + T(Kr)\right] , \tag{3.7}$$

where

$$d_0 = \frac{2\mathrm{i}}{\pi}\sum_{m=0}^{\infty}(-)^m \epsilon_m c_m , \tag{3.8}$$

$$d_m = (-)^{m+1} m(c_{m+1} - c_{m-1}) \quad (m \geqslant 1), \tag{3.9}$$

and

$$T(Kr) = \sum_{m=1}^{\infty} d_m(Ka)\, H_m R_m . \tag{3.10}$$

The reduction from (2.10) to (3.7) is particularly useful in regard to the asymptotic form for $Kr \gg 1$. Both (3.6) and the more general form of the 'quadratic forcing function' on the right-hand side of (3.2) involve sums of products of Bessel and

Hankel functions, with each product inversely proportional to $1/Kr$. Since $T(Kr)$ is of the same form, the simple first term in (3.7) is the leading-order contribution for $Kr \gg 1$, and the remaining contribution which involves products of Bessel and Hankel functions is of order $1/(Kr)^2$.

If $Kr \gg 1$ and the asymptotic approximation is substituted for the Hankel function, the scattering potential on the free surface in the reflected direction $\theta = \pi$ is equal to

$$\begin{aligned}\phi_s(r,\pi,0) &= -\mathrm{i}\frac{gA}{\omega}\sum_{m=0}^{\infty}\epsilon_m \mathrm{i}^m c_m H_m(Kr) \\ &\sim -\mathrm{i}\frac{gA}{\omega}\left(\frac{2}{\pi Kr}\right)^{1/2} \mathrm{e}^{-\mathrm{i}Kr+\mathrm{i}\pi/4}\sum_{m=0}^{\infty}\epsilon_m(-)^m c_m \\ &= -d_0\frac{gA}{\omega}\left(\frac{\pi}{2Kr}\right)^{1/2}\mathrm{e}^{-\mathrm{i}Kr+\mathrm{i}\pi/4}. \end{aligned} \tag{3.11}$$

In the short-wavelength regime $Ka \gg 1$ we shall show that the second-order force is proportional to d_0, and thus to the scattering amplitude of the reflected wave.

4. Solution for the second-order potential

A solution of the boundary-value problem for $\phi_2^{(1)}$ is sought using Weber transforms analogous to those in Emmerhoff & Sclavounos (1992, equation 45). For this purpose we first express $S(Kr)$ in the form

$$S(Kr) = \int_0^\infty \hat{S}(k) W_1(ka,kr)\frac{k\mathrm{d}k}{J_1'(ka)^2 + Y_1'(ka)^2}, \tag{4.1}$$

where

$$\hat{S}(k) = \int_a^\infty S(Kr) W_1(ka,kr)\, r\mathrm{d}r \tag{4.2}$$

and

$$W_1(ka,kr) = Y_1'(ka)J_1(kr) - J_1'(ka)Y_1(kr). \tag{4.3}$$

The solution of (3.4) is then constructed in the form

$$\phi_2^{(1)}(r,z) = \int_0^\infty \hat{\phi}_2^{(1)}(k)\,\mathrm{e}^{kz} W_1(ka,kr)\frac{k\mathrm{d}k}{J_1'(ka)^2 + Y_1'(ka)^2}, \tag{4.4}$$

where

$$\hat{\phi}_2^{(1)}(k) = \frac{4\omega K A^2 \hat{S}(k)}{k - 4K}. \tag{4.5}$$

The contour of integration in (4.4) is defined to pass above the pole $k = 4K$. This solution satisfies the homogeneous boundary condition on the cylinder, and the product of (4.4) and $\cos\theta$ satisfies the governing Laplace equation in the fluid domain. The conditions at infinity will be considered below.

The behaviour of (4.2) for small k is first determined, by considering the contribution to this integral for large values of r. From the leading term in (3.7) it follows that

$$\hat{S}(k) \sim \frac{d_0}{K}\int_a^\infty W_1(ka,kr)\,\mathrm{d}r = \frac{2d_0}{\pi K a^2}k^{-3}. \tag{4.6}$$

Substituting this result in (4.5),

$$\hat{\phi}_2^{(1)}(k) \sim -\frac{2d_0\omega A^2}{\pi K a^2} k^{-3}. \tag{4.7}$$

Thus the contribution to (4.4) from the vicinity of the lower limit $k = 0$ is

$$-\frac{2\omega A^2 d_0}{\pi K a^2} \int_0 \mathrm{e}^{kz} W_1(ka, kr) \frac{k^{-2}\mathrm{d}k}{J_1'(ka)^2 + Y_1'(ka)^2}. \tag{4.8}$$

When $r = O(a)$ the small-k expansion of the Bessel functions in (4.8) is straightforward, and it follows from Watson's lemma that the asymptotic form of (4.8) for large $|z|$ is of order $1/z^2$. Thus the solution (4.4) vanishes at large depths in an appropriate manner. Note however that while this statement applies to the first Fourier component it does not apply to the complete potential ϕ_2, which for large depths is given by the approximation

$$\phi_2 \sim -\tfrac{1}{2} d_0 \left(\frac{gA^2}{\omega}\right) \left(\frac{z}{R(R+x)}\right), \tag{4.9}$$

as shown by Newman (1990). Here $R = (x^2 + y^2 + z^2)^{1/2}$.

In the complementary case where $r \gg a$ and $|z| = O(a)$, the asymptotic approximation of (4.4) includes two contributions associated respectively with the vicinity of the lower limit $k = 0$ and with the residue from the pole at $k = 4K$. The first contribution can be evaluated from Watson's Lemma, neglecting the first term in the denominator of (4.5) and the exponential factor e^{kz} in the integrand; after recalling (4.1) this contribution is simply proportional to the forcing function on the free surface. The contribution from the residue at the pole is an outgoing radiated wave, which is analysed in the same manner as the far-field asymptotic approximation of the first-order solution (cf. Emmerhoff & Sclavounos 1992, equations 50–52). The complete asymptotic approximation of (4.4) is

$$\phi_2^{(1)} \sim -\omega A^2 S(Kr) - \frac{2\omega A^2 K}{H_1'(4Ka)} \hat{\phi}_2^{(1)}(4K) \left(\frac{2\pi}{Kr}\right)^{1/2} \mathrm{e}^{4Kz - 4\mathrm{i}Kr - (3\pi\mathrm{i}/4)}. \tag{4.10}$$

The two terms in (4.10) correspond respectively to the 'locked' and 'free' waves described by Molin (1979) and also by Mei (1983, §12.10). This confirms that the appropriate conditions at infinity are satisfied by the solution (4.4). This far-field asymptotic analysis can be generalized for the other Fourier harmonics of the second-order potential (3.3), with similar results.

5. The force due to the second-order potential

The contribution from the solution $\phi_2^{(1)}$ to the force (2.5) is a distributed force where the differential wave load per unit depth is

$$F_p' = 2\rho\mathrm{i}\omega a \int_0^{2\pi} \phi_2 \cos\theta \mathrm{d}\theta = 2\pi\mathrm{i}\omega\rho a \phi_2^{(1)}. \tag{5.1}$$

Substituting (4.4) gives the result

$$F_p' = 4\mathrm{i}\omega\rho \int_0^{\infty} \hat{\phi}_2^{(1)}(k)\, \mathrm{e}^{kz} \frac{\mathrm{d}k}{J_1'(ka)^2 + Y_1'(ka)^2}, \tag{5.2}$$

where the Wronskian has been used to simplify the integrand. Integrating vertically over the infinite depth of the cylinder gives the total force

$$F_p = 4i\omega\rho \int_0^\infty \hat{\phi}_2^{(1)}(k) \frac{k^{-1}dk}{J_1'(ka)^2 + Y_1'(ka)^2}$$
$$= 16i\rho g K^2 A^2 \int_0^\infty \frac{\hat{S}(k)}{k - 4K} \frac{k^{-1}dk}{J_1'(ka)^2 + Y_1'(ka)^2}. \tag{5.3}$$

Except for changes in notation and the simplified form (3.7) of the forcing function S, (5.3) is equivalent to the corresponding formula of Hunt & Baddour (1981).

Substituting (4.2), interchanging the orders of integration, and adopting the non-dimensional notation (1.2),

$$\bar{F}_p = 4iK/a \int_a^\infty G(Kr)S(Kr)r dr, \tag{5.4}$$

where

$$G(Kr) = 4K \int_0^\infty \frac{W_1(ka, kr)}{k - 4K} \frac{k^{-1}dk}{J_1'(ka)^2 + Y_1'(ka)^2}. \tag{5.5}$$

The integral in (5.5) can be transformed by contour integration in the complex k-plane. For this purpose we use the identity

$$\frac{W_1(ka, kr)}{J_1'(ka)^2 + Y_1'(ka)^2} = \frac{1}{2i}\left[\frac{H_1(kr)}{H_1'(ka)} - \frac{H_1^{(1)}(kr)}{H_1^{(1)'}(ka)}\right], \tag{5.6}$$

where $H_1^{(1)} = J_1 + iY_1$ is the first-kind Hankel function. After deforming the contour of integration in (5.5) to the positive or negative imaginary axes, respectively, for the terms which involve $H_1^{(1)}$ and H_1, it follows that

$$G(Kr) = \int_0^\infty \frac{K_1(4Krv)dv}{vK_1'(4Kav)(v^2 + 1)} - \pi \frac{H_1(4Kr)}{H_1'(4Ka)}$$
$$\equiv g(Kr) - \pi \frac{H_1(4Kr)}{H_1'(4Ka)}. \tag{5.7}$$

Here $g(Kr)$ denotes the integral in (5.7), and the new integration variable is defined by $k = \pm i4Kv$; the term involving the Hankel function of the second kind is due to the residue from the pole.

The function $g(Kr)$ is negative, with monotonic decreasing absolute value as Kr increases. For small values of Ka and Kr the Bessel function K_1 and its derivative can be approximated by their leading terms, giving the approximation

$$g(Kr) \sim -\frac{4}{Kr}(Ka)^2 \int_0^\infty \frac{dv}{v^2 + 1} = -\frac{2\pi(Ka)^2}{Kr}. \tag{5.8}$$

For large values of Kr the principal contribution to (5.7) is from the vicinity of the lower limit of integration. After approximating the denominator for small values of v,

$$g(Kr) \sim -(4Ka)^2 \int_0^\infty K_1(4Krv)v dv = -\frac{\pi a^2}{2r^2}. \tag{5.9}$$

In the form (5.7) the function G is essentially the same as the assisting potential derived by Lighthill (1979, equation 75) and applied to the second-order force by Eatock Taylor & Hung (1987, equation A14).

After substituting (3.7) and (5.7) in (5.4),

$$\bar{F}_p = \frac{4id_0}{a}\int_a^\infty G(Kr)\mathrm{d}r + 4\mathrm{i}/a\int_a^\infty g(Kr)T(Kr)\mathrm{d}r - 4\pi\mathrm{i}/a\int_a^\infty \frac{H_1(4Kr)}{H_1'(4Ka)}T(Kr)\mathrm{d}r. \quad (5.10)$$

The contributions from each of the three integrals in (5.10) will be considered separately, with the definitions $\bar{F}_p = \bar{F}_p^{(1)} + \bar{F}_p^{(2)} + \bar{F}_p^{(3)}$.

The first integral in (5.10), which is associated with the term d_0/Kr in (3.7), can be integrated directly to give the result

$$\bar{F}_p^{(1)} = \frac{4id_0}{a}\int_a^\infty G(Kr)\mathrm{d}r = \mathrm{i}\frac{d_0}{Ka}\int_0^\infty \frac{K_0(4Kau)\mathrm{d}u}{u^2K_1'(4Kau)(u^2+1)} - \pi\mathrm{i}\frac{d_0}{Ka}\frac{H_0(4Ka)}{H_1'(4Ka)}. \quad (5.11)$$

The contribution from the second integral is

$$\bar{F}_p^{(2)} = \frac{4\mathrm{i}}{Ka}\int_{Ka}^\infty g(u)T(u)\mathrm{d}u, \quad (5.12)$$

where the non-dimensional variable of integration is $u = Kr$. With the same change of variable, the contribution from the third integral is

$$\bar{F}_p^{(3)} = -\frac{4\pi\mathrm{i}}{KaH_1'(4Ka)}\int_{Ka}^\infty H_1(4u)T(u)\mathrm{d}u. \quad (5.13)$$

This decomposition of F_p into three separate components is effective from the computational standpoint. The component (5.11) is relatively simple to evaluate by numerical integration since the integrand is monotonic and tends to zero for large u in proportion to u^{-4}. The component (5.12) is the most difficult since the infinite series (3.10) must be summed to evaluate $T(u)$, and (5.7) must be integrated numerically to evaluate $g(u)$; for large u the integrand is oscillatory, with its modulus proportional to u^{-3}.

The component (5.13) can be evaluated more easily after deforming the contour of integration so that the integrand converges exponentially at infinity. The integrand is an analytic function of u in the complex plane, excluding a branch cut on the negative real axis. An effective contour for numerical integration is along the positive real axis from Ka to u_0, and then parallel to the negative imaginary axis from u_0 to $u_0 - \mathrm{i}\infty$. The latter component of the integral converges exponentially. The segment along the real axis is required to avoid cancellation errors associated with the fact that in the series representation (3.10) for $T(u)$, $H_m(u)$ is large, proportional to u^{-m}, when $m \gg u$. The series in (3.10) can be truncated after the term $m = M = [2Ka + 5]$. Having established this upper limit for the order of the Bessel and Hankel functions, the value of u_0 is set equal to $0.75M$. One of the advantages of the reduction from (2.10) to (3.7) is that the truncation of (3.10) can be fixed, whereas in (2.10) the maximum order M must be increased as the variable of integration $u = Kr$ is increased.

The force F_p is shown in figure 2, based on computations from a program which is intended to give final results having an absolute accuracy of at least 8 decimal places. The Bessel and Hankel functions are evaluated using Chebyshev approximations, as described at the end of §2. The series in (3.8) and (3.10) are summed directly, retaining sufficient terms to give the above accuracy. The integrals in (5.7), (5.11),

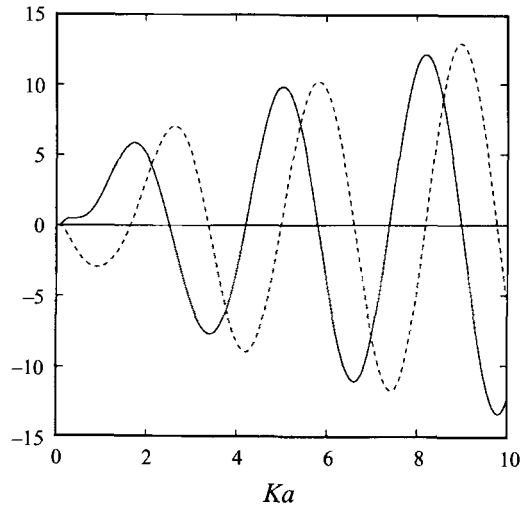

FIGURE 2. Real (solid) and imaginary (dashed) parts of the force $\bar{F}_p$ due to the second-order potential, computed from (5.11)–(5.13).

(5.12), and (5.13) are evaluated using adaptive Romberg integration in finite steps, and proceeding until the contribution from the last step is less than the prescribed tolerance for numerical error. The oscillatory behaviour which is evident in figure 2 will be discussed in §7.

6. Long-wavelength approximations

For $Ka \ll 1$ the force F_q due to the first-order potential can be approximated in a straightforward manner, using the ascending series for the Bessel functions. The leading-order contributions, of order (Ka), are from the terms $m = 0, 1$ in (2.14). The next terms in the asymptotic expansion, of order $(Ka)^3$ and $(Ka)^3 \log(Ka)$, are from the terms $m = 0, 1, 2$. After some algebra the non-dimensional force component due to the first-order potential is approximated in the form

$$\bar{F}_q = \frac{5\pi \mathrm{i}}{4} Ka \left[1 + \tfrac{1}{10}(Ka)^2 \left(\log(\tfrac{1}{2}Ka) + \gamma - \tfrac{33}{4} + \tfrac{1}{2}\pi \mathrm{i}\right)\right] + O((Ka)^5 (\log Ka)^2). \quad (6.1)$$

Figure 3 shows a comparison of (6.1) with the exact results in the range $0 < Ka < 0.5$. The long-wavelength approximation (6.1) is useful throughout this range. The leading-order term in (6.1), denoted by the short dashed line in figure 3, was derived by Lighthill (1979).

A more extensive analysis is required for the force F_p. The Bessel functions in (5.11) can be expanded in ascending series, and integrated to give the approximation

$$\bar{F}_p^{(1)} \sim -12\pi \mathrm{i} (Ka)^3 \left[\log 2Ka + \gamma + \pi \mathrm{i}\right] . \quad (6.2)$$

In the analysis of (5.12) we consider first the function $g(u)$ defined by (5.7). After expanding K_1' and retaining the leading term for small values of the argument,

$$rlg(u) \sim -(4Ka)^2 \int_0^\infty \frac{K_1(4uv) v \mathrm{d}v}{(v^2+1)}$$

$$= 4(\pi Ka)^2 \left[\mathbf{H}_{-1}(4u) - Y_{-1}(4u)\right] = (\pi Ka)^2 \frac{\mathrm{d}}{\mathrm{d}u} \left[\mathbf{H}_0(4u) - Y_0(4u)\right] , \quad (6.3)$$

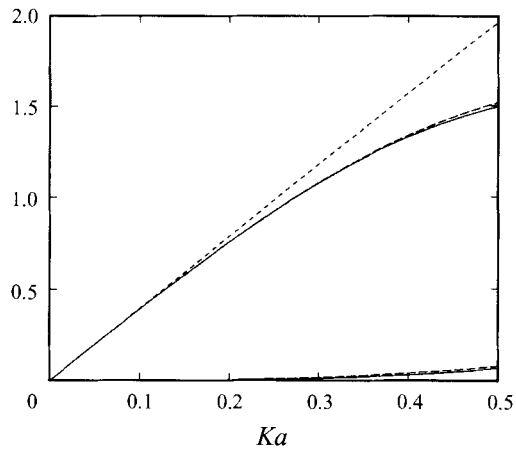

FIGURE 3. Comparison of the long-wavelength approximation (6.1) (long-dashed curves) with the 'exact' force $\bar{F}_q$ computed from (2.14) (solid curves). The real parts are shown by the two lower curves with the sign reversed. The leading-order approximation of Lighthill (1979) corresponding to the first term in (6.1) is indicated by the short-dashed line.

where $\mathbf{H}_n$ is the Struve function and the integral has been evaluated using equation (11.4.47) of Abramowitz & Stegun (1964). For $u \ll 1$ the Bessel function $Y_{-1} = Y_1$ is dominant, and

$$g(u) \sim -2\pi(Ka)^2/u, \tag{6.4}$$

in accordance with (5.8). Conversely, for $u \gg 1$, equation (12.1.34) of Abramowitz & Stegun (1964) is applicable and $g = O(u^{-2})$ in accordance with (5.9).

The product $R_m H_m$ in (3.10) is considered next, in the form

$$R_m(u)H_m(u) = J_m(u)H_m(u) - c_m H_m(u)^2. \tag{6.5}$$

For $Ka \ll 1$ it follows from the expansion of (2.4) that

$$c_0 \sim -\frac{\pi i}{4}(Ka)^2, \quad c_1 \sim \frac{\pi i}{4}(Ka)^2, \quad c_2 \sim \frac{\pi i}{32}(Ka)^4, \tag{6.6}$$

and more generally, for $m > 0$, $c_m = O((Ka)^{2m})$. Thus for $u \geqslant Ka$ each term in (6.5) is bounded, of order one as $Ka \to 0$. From (3.9) it also follows that

$$d_1 \sim \frac{\pi i}{4}(Ka)^2, \quad d_2 \sim \frac{\pi i}{2}(Ka)^2, \tag{6.7}$$

and for $m > 1$, $d_m = O((Ka)^{2m-2})$. Only the terms $m = 1$ and $m = 2$ contribute to leading order in (5.12), with the result

$$\bar{F}_p^{(2)} \sim -4\pi^3(Ka)^3 \sum_{m=1}^{2} m \int_{Ka}^{\infty} [\mathbf{H}_{-1}(4u) - Y_{-1}(4u)] \left[J_m(u)H_m(u) - c_m H_m(u)^2\right] du. \tag{6.8}$$

The contribution in (6.8) from the product $J_m H_m$ extends over the complete range $Ka < u < \infty$, with the integrand proportional to $1/u$ for $u \to Ka$. Note that

$$J_m(u)H_m(u) \sim -iJ_m(u)Y_m(u) \sim \frac{i}{\pi m} + O(u^2 \log u) \tag{6.9}$$

for $u \ll 1$, and $J_m H_m = O(1/u)$ for $u \gg 1$. After using the last form of (6.3) and

integrating by parts, this contribution to (6.8) is replaced by

$$\pi^3(Ka)^3 \int_{Ka}^{\infty} [\mathbf{H}_0(4u) - Y_0(4u)] \frac{\mathrm{d}}{\mathrm{d}u} [J_1(u)H_1(u) + 2J_2(u)H_2(u)]\, \mathrm{d}u$$
$$+\pi^3(Ka)^3 [\mathbf{H}_0(4Ka) - Y_0(4Ka)] [J_1(Ka)H_1(Ka) + 2J_2(Ka)H_2(Ka)]$$
$$\sim \pi^3(Ka)^3 \int_0^{\infty} [\mathbf{H}_0(4u) - Y_0(4u)] \frac{\mathrm{d}}{\mathrm{d}u} [J_1(u)H_1(u) + 2J_2(u)H_2(u)]\, \mathrm{d}u$$
$$-4\pi \mathrm{i}(Ka)^3 [\log(2Ka) + \gamma] \,. \tag{6.10}$$

Here (6.9) has been used to evaluate the contribution from the lower limit of integration.

Next consider the contribution in (6.8) from the products $c_m H_m^2$. Since the coefficients c_1 and c_2 are proportional to $(Ka)^{2m}$, these products only contribute to the integral in the vicinity of the lower limit of integration, where $u \ll 1$. Using (6.4), (6.6), and approximating the Hankel functions for $u \ll 1$,

$$-4\pi^3(Ka)^3 \sum_{m=1}^{2} m \int_{Ka}^{\infty} [\mathbf{H}_{-1}(4u) - Y_{-1}(4u)] \left[-c_m H_m(u)^2\right] \mathrm{d}u$$
$$\sim 2\pi \mathrm{i}(Ka)^3 \int_{Ka}^{\infty} \left[\frac{(Ka)^2}{u^2} + \frac{(Ka)^4}{u^4}\right] \frac{\mathrm{d}u}{u} = \tfrac{3}{2}\pi \mathrm{i}(Ka)^3 \,. \tag{6.11}$$

Adding (6.10) and (6.11) gives the leading-order approximation of (6.8) in the form

$$\bar{F}_p^{(2)} \sim -4\pi \mathrm{i}(Ka)^3 \left[\log(2Ka) + \gamma - \tfrac{3}{8}\right] + (Ka)^3 C^{(2)} , \tag{6.12}$$

where $C^{(2)}$ is a complex constant, equal to the factor of $(Ka)^3$ in the third line of (6.10). This constant can be expressed in the more convenient form

$$C^{(2)} = 2\pi^2 \int_0^{\infty} [\mathbf{L}_0(4v) - I_0(4v)] \frac{\mathrm{d}}{\mathrm{d}v} [I_1(v)K_1(v) + 2I_2(v)K_2(v)]\, \mathrm{d}v$$
$$+4\pi \mathrm{i} \int_0^{\infty} K_0(4v) \frac{\mathrm{d}}{\mathrm{d}v} [I_1(v)K_1(v) + 2I_2(v)K_2(v)]\, \mathrm{d}v \,, \tag{6.13}$$

which is derived by contour integration, with the new variable $v = \mathrm{i}u$, after noting that the integrand is analytic for $\mathrm{Re}(u) > 0$ and of order u^{-3} at infinity. Here $\mathbf{L}_0$ denotes the modified Struve function. The integrals in (6.13) have been evaluated by numerical integration, with the result

$$C^{(2)} = 2.534331 - 0.612503\mathrm{i} \,. \tag{6.14}$$

Proceeding in a similar manner for $F_p^{(3)}$, defined by (5.13), (6.3) is replaced by

$$-\pi \frac{H_1(4u)}{H_1'(4Ka)} \sim -8\pi^2 \mathrm{i}(Ka)^2 H_1(4u) \sim 4\pi(Ka)^2/u \,, \tag{6.15}$$

where the last approximation is valid for $u \ll 1$. Thus

$$\bar{F}_p^{(3)} \sim 8\mathrm{i}\pi^3(Ka)^3 \sum_{m=1}^{2} m \int_{Ka}^{\infty} H_1(4u) \left[J_m(u)H_m(u) - c_m H_m(u)^2\right] \mathrm{d}u \,. \tag{6.16}$$

The contribution to (6.16) from the terms $J_m H_m$ can be approximated in the same

manner as (6.10) to give the result

$$-2\mathrm{i}\pi^3(Ka)^3\int_{Ka}^{\infty}H_1(4u)\frac{\mathrm{d}}{\mathrm{d}u}\left[J_1(u)H_1(u)+2J_2(u)H_2(u)\right]\mathrm{d}u$$
$$-2\mathrm{i}\pi^3(Ka)^3H_1(4Ka)\left[J_1(Ka)H_1(Ka)+2J_2(Ka)H_2(Ka)\right]$$
$$\sim +8\pi\mathrm{i}(Ka)^3\left[\log(2Ka)+\gamma+\frac{1}{2}\pi\mathrm{i}\right]+8\mathrm{i}\pi(Ka)^3C^{(3)} \tag{6.17}$$

where

$$C^{(3)}=\frac{\pi^2}{4}\int_0^{\infty}H_0(4u)\frac{\mathrm{d}}{\mathrm{d}u}\left[J_1(u)H_1(u)+2J_2(u)H_2(u)\right]\mathrm{d}u$$
$$=-\int_0^{\infty}K_0(4v)\frac{\mathrm{d}}{\mathrm{d}v}\left[I_1(v)K_1(v)+2I_2(v)K_2(v)\right]\mathrm{d}v\,. \tag{6.18}$$

The last form of this integral is derived as in (6.13), and it follows from numerical integration that

$$C^{(3)}=-\frac{1}{4\pi}\mathrm{Im}\left(C^{(2)}\right)=0.048741\,. \tag{6.19}$$

Since the last approximation in (6.15) differs from (6.4) by the simple factor -2, the same factor can be multiplied by (6.11) to obtain the result

$$8\mathrm{i}\pi^3(Ka)^3\sum_{m=1}^{2}m\int_{Ka}^{\infty}H_1(4u)\left[-c_mH_m(u)^2\right]\mathrm{d}u\sim-3\pi\mathrm{i}(Ka)^3\,. \tag{6.20}$$

Adding the contributions (6.17) and (6.20) gives

$$\bar{F}_p^{(3)}\sim 8\pi\mathrm{i}(Ka)^3\left[\log(2Ka)+\gamma-\tfrac{3}{8}+\tfrac{1}{2}\pi\mathrm{i}+C^{(3)}\right]\,. \tag{6.21}$$

The total force component $\bar{F}_p$ due to the second-order potential can be approximated by the sum of (6.2), (6.12) and (6.21), with the final result

$$\bar{F}_p\sim-8\pi\mathrm{i}(Ka)^3(\log 2Ka+\gamma)+(Ka)^3\left[81.39117+0.612503\mathrm{i}\right]\,. \tag{6.22}$$

Neglecting a logarithmic factor, the error in this approximation is of order $(Ka)^5$. Figure 4 shows a comparison of (6.22) with the exact results in the range $0<Ka<0.5$. The long-wavelength approximation (6.22) is useful only for values of Ka less than 0.1–0.15.

Figure 5 compares the long-wavelength approximation with the exact results for the total force F_p+F_q, with a similar conclusion regarding the validity of the approximate results as in the discussion pertaining to F_p in the preceding paragraph.

The long-wavelength approximations (6.1) and (6.22) have been derived directly from the exact expressions for the second-order forces. These approximations are valid only for the specific case of an infinitely deep cylinder. An alternative approach is to approximate the velocity potential near the body, as in Lighthill (1979). The latter approach is simpler, and more easily extended to other bodies. However it does not yield the same results as in (6.1) and (6.22). With respect to the force $\bar{F}_q$ due to the first-order potential, Lighthill (1979) derives only the leading-order term in (6.1) proportional to Ka. With respect to the force $\bar{F}_p$ due to the second-order potential, Lighthill (1979) derives an approximation similar in form to (6.22) but with the imaginary factor $-\frac{3}{2}\pi\mathrm{i}$ in place of the complex constant in square brackets in (6.22). (The exact value of this factor is not explicit in Lighthill (1979), but it is

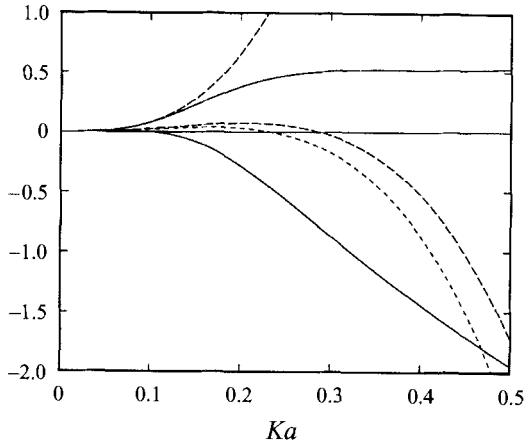

FIGURE 4. Comparison of the long-wavelength approximation (6.22) (long-dashed curves) with the 'exact' force $\bar{F}_p$ computed from (5.11)–(5.13) (solid curves). The real parts are the two upper curves. The approximation derived by Lighthill (1979) for the imaginary component is indicated by the short-dashed curve.

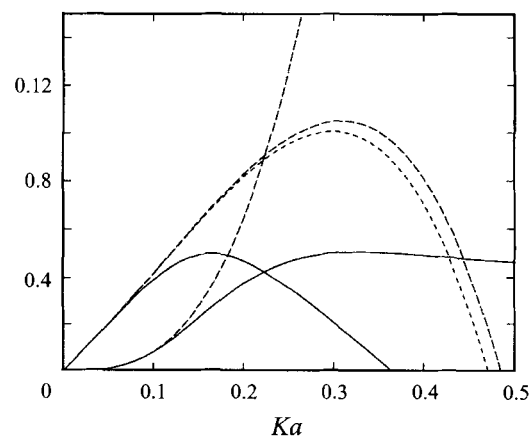

FIGURE 5. Comparison of the long-wavelength approximation for the total second-order force $F_p + F_q$ (long-dashed curves) with the corresponding 'exact' computed results (solid curves). The real parts are the two curves tangent to the horizontal axis at the origin. The approximation derived by Lighthill (1979) for the imaginary component is indicated by the short-dashed curve.

implied there and confirmed by Eatock Taylor & Hung (1987) who compare it with their numerical results.) Lighthill's analysis is restricted to the solution near the body, and the argument which is used to estimate the integral over the free surface far from the body appears to be incomplete.

The approximations of Lighthill (1979) are included in figures 3–5 for comparison. For the component $\bar{F}_q$ shown in figure 3, the more complete approximation (6.1) is useful over a substantially larger range. For the imaginary part of the component $\bar{F}_p$ the distinction between Lighthill's factor and the corresponding imaginary constant in (6.22) is relatively unimportant, and in fact Lighthill's approximation is somewhat closer to the exact computed results. However the real component in (6.22) is more important in the range $Ka < 0.15$, and for larger values of Ka both approximations for F_p are essentially useless.

7. Short-wavelength approximations

In the short-wavelength regime ($Ka \gg 1$) the first-order diffraction field near the cylinder can be approximated by the method of geometric optics. In the 'illuminated' region on the upwave side of the cylinder the potential ϕ_1 consists of the incident wave plus a reflected wave with the same amplitude and phase on the cylinder:

$$\phi_1 \sim 2(igA/\omega)\, e^{Kz - iKa\cos\theta} \quad \text{for } (\pi/2 < \theta < 3\pi/2). \tag{7.1}$$

In the 'shadow region' on the downwave side the potential vanishes. Using these results to evaluate the tangential velocity components on the cylinder, it follows from (2.9) and the boundary condition $\phi_{1r} = 0$ that

$$S(Ka) \sim \frac{i}{\pi} \int_{\pi/2}^{3\pi/2} e^{-2iKa\cos\theta} \cos^3\theta \, d\theta \sim -(\pi Ka)^{-1/2} e^{2iKa + \pi i/4}, \tag{7.2}$$

where the method of stationary phase is used to approximate the last integral.

Considering first the force F_q due to the first-order potential, the distributed force (2.7) can be evaluated directly using (7.2), and the point force (2.8) can be approximated in a similar manner using (7.1) to evaluate the free-surface elevation ζ. It follows that

$$\bar{F}_q \sim -\tfrac{3}{2} i \left(\frac{\pi}{Ka}\right)^{1/2} e^{2iKa + \pi i/4}. \tag{7.3}$$

For the force F_p, the dominant contribution for $Ka \gg 1$ is from the component (5.11). The last integral in (5.11) can be approximated by neglecting the factor $1 + u^2$ in the denominator and changing the variable of integration. It follows that this integral is proportional to Ka, and dominant by comparison to the residue term. Thus

$$\bar{F}_p^{(1)} \sim 4i d_0 \int_0^\infty \frac{K_0(v)dv}{v^2 K_1'(v)}. \tag{7.4}$$

From the asymptotic expansions for J_m and H_m it follows that $c_m = O(1)$, for $Ka \gg m$, and $c_m \to 0$ for $m \gg Ka$. The coefficients d_m have a similar behaviour, with the exception of the sum d_0 which can be approximated from (3.7) and (7.2) in the following manner. First note that the series (3.10) is of order $1/Ka$, and thus the first term on the right-hand side of (3.7) is dominant. After setting $r = a$ it follows that

$$d_0 \sim KaS(Ka) \sim -\left(\frac{Ka}{\pi}\right)^{1/2} e^{2iKa + \pi i/4}, \tag{7.5}$$

where (7.2) has been used in the last approximation. The same result may be derived from the more complicated asymptotic analysis described by Jones (1964, §8.7, equation 36).

The integral in (7.4) is equal to a real constant with the value -1.85463, based on numerical integration. Using (7.5) it follows that

$$\bar{F}_p \sim 4.185i\,(Ka)^{1/2} e^{2iKa + \pi i/4}. \tag{7.6}$$

Since the first-order diffraction field is concentrated near the free surface, the force F_q is relatively small. The second-order potential is attenuated more slowly with depth, and thus the corresponding force (7.6) is dominant. For depths z which are large compared to both the wavelength and cylinder radius (4.9) can be integrated over the cylinder to give the same result as (7.6), but with the smaller constant factor $2\pi^{1/2} = 3.545$ in place of 4.185. This difference can be attributed

Ka	F_q/F_{qa}		F_p/F_{pa}	
	Re	Im	Re	Im
2	0.7474	0.3535	0.9058	0.4613
4	0.9931	0.3437	1.0317	0.2755
6	0.8901	0.2636	1.0041	0.1918
8	0.9550	0.0990	1.0089	0.1178
10	1.0334	0.1445	1.0260	0.1017
12	0.9559	0.1428	1.0109	0.0925
14	0.9807	0.0590	1.0087	0.0673
16	1.0229	0.0933	1.0167	0.0624
18	0.9728	0.0920	1.0087	0.0596
20	0.9927	0.0436	1.0078	0.0471

TABLE 1. Ratios of the exact values of the second-order force components divided by their asymptotic approximations F_{qa} and F_{pa}, defined respectively by (7.3) and (7.6).

to the use of the far-field approximation for the free-surface forcing function in (4.9), with the consequence that this approximation is not accurate close to the free surface.

Table 1 shows the ratios between the 'exact' numerical evaluations of F_q and F_p and the corresponding short-wavelength approximations (7.3) and (7.6). These approximations have relative accuracies within a few percent for the modulus when $Ka > 3$. Approximations which have a similar accuracy for both the modulus and phase result if (7.3) and (7.6) are multiplied by the factor $(1 + \mathrm{i}/Ka)$; this factor has been determined empirically from the results in table 1, and not by a higher-order asymptotic analysis.

8. Finite depth

For a fluid of finite depth h, with the cylinder extending from the free surface to the bottom at $z = -h$, the first-order diffraction potential (2.2) is replaced by the corresponding solution

$$\phi_1 = \frac{\mathrm{i}gA}{\omega} \frac{\cosh(K(z+h))}{\cosh(Kh)} \sum_{m=0}^{\infty} \epsilon_m \mathrm{i}^{-m} \cos m\theta \, R_m(Kr), \tag{8.1}$$

where the frequency ω and wavenumber K are related by the dispersion relation

$$\frac{\omega^2}{g} \equiv \nu = K \tanh Kh. \tag{8.2}$$

The appropriate modifications of the force F_q due to the first-order potential are relatively simple, with the result that (2.14) is replaced by

$$\bar{F}_q = -\frac{2\mathrm{i}}{\pi(Ka)^2} \sum_{m=0}^{\infty} (-)^m \left(\frac{1}{H'_m H'_{m+1}} \right) \times \left[3 + \frac{m(m+1)}{K^2a^2} - \frac{2Kh}{\sinh 2Kh} \left(1 - \frac{m(m+1)}{K^2a^2} \right) \right]. \tag{8.3}$$

The contribution from the last pair of terms in square brackets, which represents

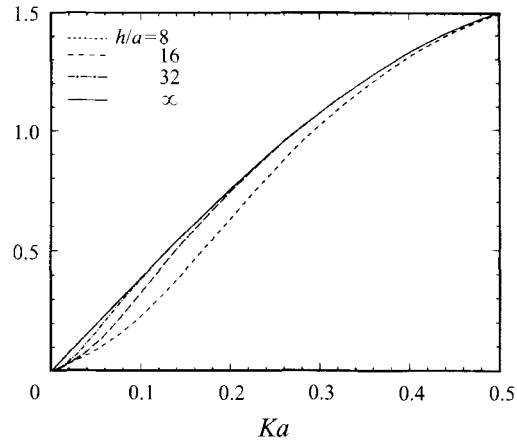

FIGURE 6. Imaginary part of the force $\bar{F}_q$ computed from (8.3). (The corresponding results for the real part of $\bar{F}_q$ are graphically indistinguishable from the infinite-depth limit shown in figure 3.) The different curves correspond to increasing depths $h/a = 8, 16, 32, \infty$ as shown in the legend.

the difference between (8.3) and (2.14), is exponentially small for $Kh \gg 1$. Figure 6 shows computations based on (8.3) for increasing values of the depth, to indicate the correlation with the infinite-depth limit. For small values of Ka the imaginary component is affected by the depth, but the real component is small and insensitive to the depth. For $Ka \ll 1$ and $Kh \ll 1$, the slope of the imaginary component is reduced by the factor 2/5.

The second-order potential is forced by the inhomogeneous free-surface condition analogous to (3.2), which now includes additional terms on the right-hand side:

$$4\nu\phi_2 - \phi_{2z} = \frac{\mathrm{i}\omega}{g}\left[\nabla\phi_1 \cdot \nabla\phi_1 + \tfrac{1}{2}\phi_1(\nu\phi_{1z} - \phi_{1zz})\right]_{z=0}. \tag{8.4}$$

After expanding the potential ϕ_2 in a Fourier series, as in (3.3), the relevant component satisfies a free-surface condition analogous to (3.4), in the form

$$4\nu\phi_2^{(1)} - \phi_{2z}^{(1)} = -\frac{4gK^2A^2}{\omega}\left[S(Kr) - \tfrac{3}{2}\operatorname{sech}^2 Kh \sum_{m=0}^{\infty}(-)^m R_m R_{m+1}\right]. \tag{8.5}$$

The sum in (8.5) accounts for the contribution from the extra terms in (8.4), and for the modification to the vertical gradient of the potential due to the effect of the finite depth. After substituting (2.3), and using the identity (Abramowitz & Stegun, equation 10.1.78)

$$J_1(2z) = 2\sum_{m=0}^{\infty}(-)^m J_m(z) J_{m+1}(z), \tag{8.6}$$

it follows that

$$\sum_{m=0}^{\infty}(-)^m R_m R_{m+1} = \tfrac{1}{2}J_1(2Kr) - c_0 H_0 J_1 + \sum_{m=1}^{\infty}(-)^m c_m H_m (R_{m-1} - J_{m+1}). \tag{8.7}$$

To conform with the notation of the infinite-depth case it is convenient to redefine

the forcing function on the right-hand side of (8.5) as follows:

$$4\nu\phi_2^{(1)} - \phi_{2z}^{(1)} = -\frac{4gK^2A^2}{\omega Kr}\left[d_0 + T(Kr) - \tfrac{3}{4}Kr\,\mathrm{sech}^2 Kh J_1(2Kr)\right]. \tag{8.8}$$

Here, corresponding to (3.10),

$$T(Kr) = \sum_{m=1}^{\infty} d_m(Ka)\,H_m R_m + \tfrac{3}{2}Kr\,\mathrm{sech}^2 Kh\left[c_0 H_0 J_1 - \sum_{m=1}^{\infty}(-)^m c_m H_m (R_{m-1} - J_{m+1})\right]. \tag{8.9}$$

The term in (8.7) and (8.8) involving $J_1(2Kr)$ is associated with the second-order component of the incident-wave potential. The forcing effect from this term is attenuated too slowly in the far field to be represented by a Weber transform, and it must be treated separately as described in the next section. The additional potential and force associated with the remaining terms in (8.8) are analysed in §10.

9. The force due to the second-order incident-wave potential

The contribution to the second-order solution due to the forcing from the first term on the right-hand side of (8.7) is associated with the second-order incident-wave potential, and satisfies the free-surface condition

$$4\nu\phi_{2I}^{(1)} - \phi_{2Iz}^{(1)} = \frac{3gK^2A^2}{\omega}\,\mathrm{sech}^2 Kh\,J_1(2Kr). \tag{9.1}$$

A particular solution which corresponds to the incident-wave potential alone is obtained by inspection in the form

$$\phi_{2I}^{(1)} = \frac{3gK^2A^2}{\omega\nu}\frac{\cosh(2K(z+h))}{\sinh^2 2Kh}J_1(2Kr). \tag{9.2}$$

This solution satisfies the boundary conditions except on the cylinder, and a homogeneous solution of (9.1) must be added to represent the corresponding scattering effect. The appropriate scattering solution is readily obtained from the first-order theory of Havelock (1929), in the form

$$\phi_{2S}^{(1)} = \frac{gA^2}{\omega\nu\sinh^2 Kh}\left[b_0 k_0^2 H_1(k_0 r)Z_0(z) + \sum_{n=1}^{\infty} b_n \kappa_n^2 K_1(\kappa_n r)Z_n(z)\right]. \tag{9.3}$$

Here k_0 is the positive real root of the equation

$$4\nu - k_0 \tanh k_0 h = 0, \tag{9.4}$$

and $\mathrm{i}\kappa_n$ is the set of imaginary roots of (9.4), ordered such that $(n - \frac{1}{2})\pi < \kappa_n h < n\pi$. The functions of the vertical coordinate z in (9.3) are

$$Z_0(z) = \frac{\cosh(k_0(z+h))}{\cosh k_0 h}, \qquad Z_n(z) = \frac{\cos(\kappa_n(z+h))}{\cos \kappa_n h}, \tag{9.5}$$

and K_1 is the modified Bessel function of the second kind. The coefficients b_0, b_n in (9.3) are evaluated from the boundary condition

$$\phi_{2Ir}^{(1)} + \phi_{2Sr}^{(1)} = 0 \quad (r = a), \tag{9.6}$$

and it follows from the orthogonality of (9.5) that

$$b_0 = -\frac{3K^3 J_1'(2Ka)}{2k_0^3 H_1'(k_0 a)} \frac{\cosh k_0 h}{\cosh^2 Kh} \left[1 + \frac{\sinh 2k_0 h}{2k_0 h}\right]^{-1} \times \left[\frac{\sinh(k_0 + 2K)h}{(k_0 + 2K)h} + \frac{\sinh(k_0 - 2K)h}{(k_0 - 2K)h}\right] \tag{9.7}$$

and

$$b_n = -\frac{3K^3 J_1'(2Ka)}{\kappa_n^3 K_1'(\kappa_n a)} \frac{\cos \kappa_n h}{\cosh^2 Kh} \left[1 + \frac{\sin 2\kappa_n h}{2\kappa_n h}\right]^{-1} \times \left[\frac{2K \sinh 2Kh \cos \kappa_n h + \kappa_n \cosh 2Kh \sin \kappa_n h}{(4K^2 + \kappa_n^2)h}\right]. \tag{9.8}$$

The force due to (9.2) is obtained by integrating the corresponding pressure over the cylinder, as in (5.1)–(5.3), with the result

$$\bar{F}_I^{(1)} = \tfrac{3}{2}\pi \mathrm{i} \frac{J_1(2Ka)}{\sinh^2 Kh}. \tag{9.9}$$

The additional force component due to (9.3) is

$$\bar{F}_I^{(2)} = 2\pi \mathrm{i} \left[b_0 H_1(k_0 a) - \sum_{n=1}^{\infty} b_n K_1(\kappa_n a)\right]. \tag{9.10}$$

These results are consistent with the corresponding expressions given by Kim & Yue (1989, Appendix B).

The sum of (9.9) and (9.10) is the force due to the diffraction of the second-order incident-wave potential,

$$\bar{F}_I = \tfrac{3}{2}\pi \mathrm{i} \frac{J_1(2Ka)}{\sinh^2 Kh} + \frac{8\pi \mathrm{i}}{\sinh^2 Kh} \left[b_0 H_1(k_0 a) - \sum_{n=1}^{\infty} b_n K_1(\kappa_n a)\right]. \tag{9.11}$$

For $Kh \gg 1$, $k_0 \to 4K$ and the coefficients (9.7)–(9.8) are of order one. Thus (9.11) tends to zero exponentially, in proportion to the forcing function on the right-hand side of (9.1). Conversely, in the shallow-water limit $vh \to 0$, the second-order component of the incident-wave potential is singular, and (9.11) is unbounded, with the long-wavelength approximation

$$\bar{F}_I = 3\pi \mathrm{i}(a/h)(vh)^{-1/2} + O\left((vh)^{1/2} \log(vh)\right). \tag{9.12}$$

The first two terms in (9.11) contribute equally to (9.12).

Figure 7 shows computations based on (9.11). For $va \ll 1$ the singular component (9.12) is the dominant feature of these curves. For large values of va the magnitude of F_I is negligible.

10. The force due to the second-order body potential

The remaining component of the second-order potential is associated with the contributions to the free-surface forcing function due to the first-order scattering potential, i.e. the terms $d_0 + T(Kr)$ in (8.8). Following the same procedure as in §4,

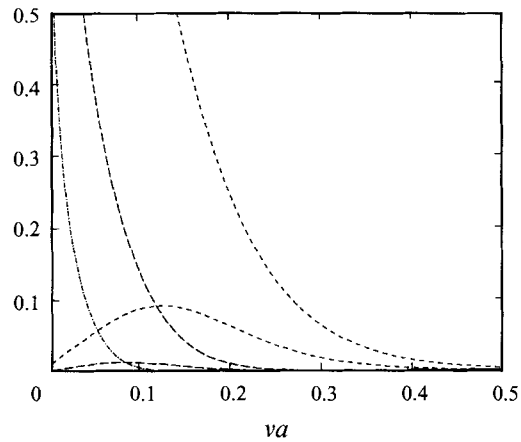

FIGURE 7. The force $\bar{F}_I$ due to the second-order component of the incident-wave potential, evaluated from (9.11), for the three finite depths $h/a = 8, 16, 32$ as shown in the legend of figure 6. The three curves which are bounded represent the real component and those which are unbounded as $va \to 0$ represent the imaginary component. (For $h/a = 32$ the imaginary component is practically zero.)

the solution can be expressed in the form

$$\phi_{2B}^{(1)}(r,z) = \int_0^\infty \hat{\phi}_2^{(1)}(k) \cosh k(z+h) \frac{W_1(ka,kr)k\mathrm{d}k}{J_1'(ka)^2 + Y_1'(ka)^2}. \tag{10.1}$$

Here the exponential function in (4.4) has been modified to satisfy the boundary condition on the bottom $z = -h$, and

$$\hat{\phi}_2^{(1)}(k) = \frac{4(g/\omega)KA^2}{k\sinh kh - 4\nu\cosh kh} \int_a^\infty [d_0 + T(Kr)]\, W_1(ka,kr)\,\mathrm{d}r. \tag{10.2}$$

Before considering the evaluation of (10.1) we proceed to integrate over the cylinder, to obtain the force F_B as in (5.1)–(5.3). The result is

$$\bar{F}_B = \frac{4\mathrm{i}}{a} \int_a^\infty G(Kr)\,[d_0 + T(Kr)]\,\mathrm{d}r, \tag{10.3}$$

where

$$G(Kr) = 2\mathrm{i}K \int_0^\infty \left[\frac{H_1^{(1)}(kr)}{H_1^{(1)'}(ka)} - \frac{H_1(kr)}{H_1'(ka)}\right] \frac{k^{-1}\sinh kh\,\mathrm{d}k}{k\sinh kh - 4\nu\cosh kh}. \tag{10.4}$$

Following the same technique as used by John (1950) to derive an eigenfunction expansion of the source potential, the range of integration in (10.4) can be extended to $-\infty \pm \mathrm{i}0$ for the two terms in square brackets, respectively, and the resulting integrals can be evaluated by summing the residues on the imaginary axis. It follows that

$$G(Kr) = \sum_{n=1}^{\infty} g_n \left[\frac{K_1(\kappa_n r)}{K_1'(\kappa_n a)}\right] - g_0 \left[\frac{H_1(k_0 r)}{H_1'(k_0 a)}\right] \equiv g - g_0 \left[\frac{H_1(k_0 r)}{H_1'(k_0 a)}\right]. \tag{10.5}$$

Here g denotes the contribution from the infinite series, which is real, with the same notation as in (5.7). The coefficients g_0 and g_n are defined by

$$g_0 = 4\pi K \frac{4\nu/k_0}{k_0^2 h + 4\nu - 16\nu^2 h}, \qquad g_n = 4\pi K \frac{4\nu/\kappa_n}{\kappa_n^2 h - 4\nu + 16\nu^2 h}. \tag{10.6}$$

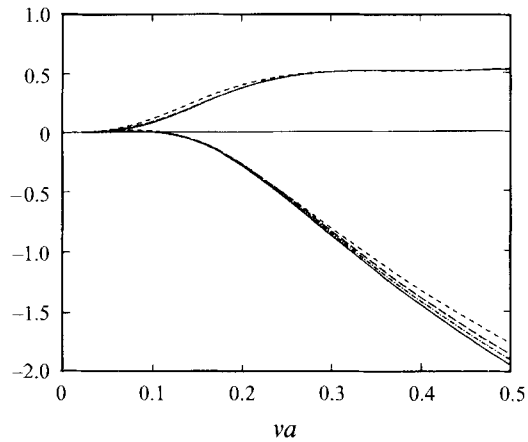

FIGURE 8. The force $\bar{F}_B$ due to the second-order component of the body potential, given by the sum of (10.7)–(10.9). The fluid depths are as in figure 6. The four upper curves represent the real component and the lower curves represent the imaginary component.

The force (10.3) may now be evaluated using (10.5). The following components are analogous to (5.11)–(5.13):

$$\bar{F}_B^{(1)} = 4\mathrm{i}(d_0/a)\int_a^\infty G(Kr)\mathrm{d}r$$

$$= 4\mathrm{i}(d_0/a)\left(\sum_{n=1}^{\infty} g_n\left[\frac{K_0(\kappa_n a)}{\kappa_n K_1'(\kappa_n a)}\right] - g_0\left[\frac{H_0(k_0 a)}{k_0 H_1'(k_0 a)}\right]\right), \tag{10.7}$$

$$\bar{F}_B^{(2)} = \frac{4\mathrm{i}}{a}\int_a^\infty g(Kr)T(Kr)\mathrm{d}r, \tag{10.8}$$

$$\bar{F}_B^{(3)} = -\frac{4\mathrm{i}g_0}{aH_1'(k_0 a)}\int_a^\infty H_1(k_0 r)T(Kr)\mathrm{d}r. \tag{10.9}$$

Computations of the force due to (10.7)–(10.9) are shown in figure 8 and compared with the infinite-depth limit evaluated from (5.11)–(5.13). The effect of finite depth is relatively small. The total force due to the combined effects of the second-order incident-wave and body potentials is shown in figure 9, and it is evident that in the long-wavelength regime the principal effect of finite depth is the singularity in the incident-wave potential represented by (9.12).

One feature to note in figures 8 and 9 is the small but persistent effect of finite depth for increasing values of va. This is in contrast to the first-order diffraction force, where the finite-depth effect is exponentially small in the same regime. Physically this difference is due to the presence of evanescent modes, and to the slow attenuation with depth of the second-order potential (4.9). More specifically, if $h/a \gg 1$ and $va \gg 1$ a short-wavelength approximation analogous to (7.6) can be derived from asymptotic analysis of (10.7) in the form

$$\bar{F}_p \sim 4.185\,[1 + 0.2696\epsilon(\log\epsilon - 1)]\,\mathrm{i}(Ka)^{1/2}\,\mathrm{e}^{2\mathrm{i}Ka + \pi\mathrm{i}/4}, \tag{10.10}$$

where $\epsilon = (\pi a/4h)$. Thus the second-order force is similar to that shown in figure 2, but with real and imaginary components reduced by the factor in square brackets in

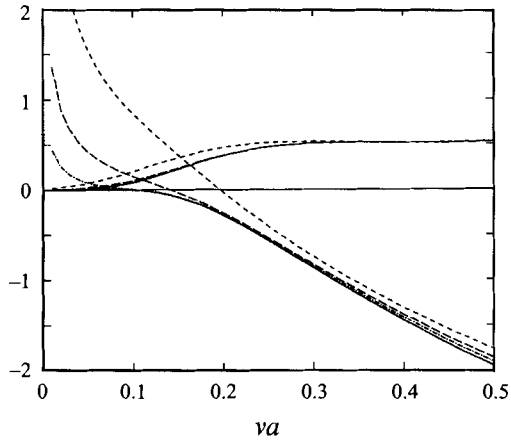

FIGURE 9. The total force $\bar{F}_p = \bar{F}_I + \bar{F}_B$ due to the second-order components of the incident-wave and body potentials which are plotted separately in figures 7 and 8. The fluid depths are as in figure 6.

(10.10). On the other hand, in the regime shown in figures 8 and 9, the finite-depth correction only affects the imaginary component of F_p since the parameter d_0 is predominantly real.

11. Discussion

A refined analysis has been made of the second-harmonic second-order force acting on a cylinder in regular waves. This consists of a component F_q due to quadratic interactions of the first-order diffraction solution, and a component F_p due to the second-order velocity potential ϕ_2. The former is relatively straightforward to evaluate, and the procedure followed here is essentially the same as in other references.

To analyse the more difficult component F_p, the relevant Fourier component of the potential ϕ_2 is derived by means of a Weber transform. The corresponding forcing function on the free surface is reduced, in the case of infinite depth, to the form (3.7) where the dominant component in the far field is inversely proportional to the radial coordinate and proportional to the back-scattered component of the first-order diffraction solution in the direction opposite to that of the incident waves. Computations of F_p are facilitated by treating the latter component separately, and also by applying contour integration to the remaining oscillatory quantities on the free surface.

As a result of these procedures it is possible to compute the second-order force with substantial accuracy, over a broad range of frequencies. Algorithms have been used which are intended to be accurate to more than 8 decimal places. Sample results are shown in table 2 to permit benchmark comparisons of other codes. We omit more detailed tabular data, but note that specific comparisons have been made with the earlier computations of Eatock Taylor & Hung (1987) and Kim & Yue (1989). The former are presented in extensive tabular form with four significant decimals included, and we find complete agreement except for a few entries which differ by only one unit in the fourth significant decimal. The results of Kim & Yue (1989), which are a special case of their more general analysis for truncated cylinders, are only slightly less accurate.

h/a	$va = 0.1$	$va = 1.0$	$va = 10$
$\bar{F}_q$:			
1	(−0.036383, 0.462130)	(−1.351504, 0.498970)	(0.768230, 0.423660)
10	(−0.001434, 0.340329)	(−0.921028, 1.178992)	(0.768230, 0.423660)
∞	(−0.000558, 0.388529)	(−0.921028, 1.178992)	(0.768230, 0.423660)
$\bar{F}_p$:			
1	(7.480456, 25.07144)	(1.585936, 0.416956)	(−6.447914, −3.261691)
10	(0.153891, 0.515222)	(2.087783, −2.655653)	(−11.50236, −5.767010)
∞	(0.080854, −0.000642)	(2.099489, −2.920977)	(−12.20275, −6.103843)
$\bar{F}_B$:			
1	(0.243202, −0.096270)	(1.792721, −0.549315)	(−6.447914, −3.261691)
10	(0.103910, 0.007397)	(2.087783, −2.655653)	(−11.50236, −5.767010)
$\bar{F}_I$:			
1	(7.237255, 25.16771)	(−0.206785, 0.966271)	(0.000000, 0.000000)
10	(0.049981, 0.507824)	(0.000000, 0.000000)	(0.000000, 0.000000)

TABLE 2. Non-dimensional force components tabulated for three values of the parameters va and h/a. In the infinite-depth limit $\bar{F}_I = 0$ and $\bar{F}_B = \bar{F}_p$.

A notable feature of the direct solution based on the Weber transforms is that the far-field asymptotic form of the second-order potential is readily derived, and shown to correspond with the description of Molin (1979) in terms of a 'free' component with outgoing waves analogous to the first-order radiated waves, and 'locked' waves which are in phase with the free-surface forcing function. In terms of the Weber integral transform for the potential over the wavenumber space k, these two components correspond respectively to the contributions from near the origin ($k = 0$), and from the residue at the pole where k is equal to the wavenumber $4K$ of a plane wave with the second-harmonic frequency 2ω.

The direct solution carried out here has been simplified substantially by considering only the first Fourier harmonic of the forcing function and the second-order potential, proportional to $\cos\theta$. This is the only component required for the evaluation of the second-order force F_p. The more complete solution including all Fourier coefficients is required for other purposes, as emphasized by Chau & Eatock Taylor (1992) in their study of the second-order free-surface elevation. The complete solution also is required for the evaluation of the third-order force, as in the work of Malenica & Molin (1995). It is straightforward to extend the solution based on Weber transforms to include the complete Fourier series, as is done formally by Hunt & Baddour (1981). The principal restriction in the context of the present analysis is that the higher harmonics of the forcing function on the free surface cannot be reduced to simple forms analogous to (3.7), and it is necessary to proceed more directly from the conventional forms analogous to (3.6).

Special attention has been given here to the asymptotic approximation of F_q and F_p for the long-wavelength regime ($Ka \ll 1$). For F_q a two-term expansion is derived which extends the corresponding result of Lighthill (1979), and gives results which are

accurate within a few percent when $Ka < 0.6$. For F_p the analysis is more complete than that given by Lighthill (1979), including both the imaginary and real components which are of comparable order. However the practical regime in which F_p can be approximated in this manner is relatively restricted, with significant departure from the exact results when Ka is between 0.1 and 0.2. A plausible explanation for this restriction, suggested by Malenica & Molin (1995), is that the relevant parameter in the expressions for F_p is $4Ka$ instead of Ka itself.

The effect of a finite fluid depth is examined, and is particularly significant when the wavelength is long relative to the depth. The dominant effect is from the second-order component of the incident wave itself, and from the corresponding scattering effect by the cylinder. The force which is due to these two relatively simple effects is singular as $Ka \to 0$. The remaining components of F_p are affected less significantly. For short wavelengths, on the other hand, the most significant modification is a small but persistent effect on F_p due to the slow attenuation of the second-order potential with depth (Newman 1990).

These conclusions regarding the long-wavelength approximation of the second-order force may have relevance in the context of the controversy between Faltinsen *et al.* (1995), and Malenica & Molin (1995). As noted in the Introduction, Faltinsen *et al.* use an extension of the long-wavelength approach ($Ka \ll 1$) to study third-order forces, assuming the wave amplitude A and cylinder radius a to be of the same order of magnitude and the depth h to be infinite. The analysis of Malenica & Molin is based on the third-order extension of the diffraction analysis used here, i.e. $Ka = O(1)$ and $A \ll a$, while h is finite. Malenica & Molin present a numerical comparison between the two theories when $a/h \ll 1$ and $Kh \gg 1$, and conclude that the Faltinsen *et al.* regime is restricted severely. The present work supports the hypothesis of Malenica & Molin that the domain of validity of the long-wavelength approximation for the second-order wave loads is only one-quarter of the corresponding domain for the first-order force, in proportion to the corresponding wavenumbers of the first- and second-harmonic waves.

Also considered in the present work is the complementary asymptotic regime of short wavelengths. Both F_q and F_p are oscillatory in phase, in the same manner as the back-scattered amplitude of the first-order diffraction problem. However the modulus of F_p increases in proportion to the square-root of Ka, whereas F_q is inversely proportional to the same factor. The relatively small magnitude of F_q can be attributed to the fact that the first-order diffraction potential is confined to an exponentially small depth near the free surface. Conversely, the pressure associated with the second-order potential is slowly attenuated with depth, and the resulting force F_p is dominant. Analogous two-dimensional results have been derived by McIver (1994), who finds for a floating body that F_p increases linearly with Ka.

This work was conducted under a Joint Industry Project sponsored by the Chevron Petroleum Technology Company, David Taylor Model Basin, Det Norske Veritas. Exxon Production Research, Mobil Oil Company, Norsk Hydro, Offshore Technology Research Center, Petrobrás, Saga Petroleum, Shell Development Company, and Statoil. Additional support was provided by the National Science Foundation Grant 9416096-CTS. Special thanks are due to Dr C.-H. Lee who provided analytical and numerical assistance, including computations with a second-order panel code which were helpful in confirming the present results.

REFERENCES

ABRAMOWITZ, M. & STEGUN, I. A. 1964 *Handbook of Mathematical Functions with Formulas, Graphs, and Mathematical Tables.* US Government Printing Office and Dover.

CHAU, F. P. & EATOCK TAYLOR, R. 1992 Second order wave diffraction by a vertical cylinder. *J. Fluid Mech.* **240**, 571–599.

EATOCK TAYLOR, R. & HUNG, S. M. 1987 Second order diffraction forces on a vertical cylinder in regular waves. *Appl. Ocean Res.* **9**, 19–30.

EMMERHOFF, O. J. & SCLAVOUNOS, P. D. 1992 The slow-drift motion of arrays of vertical cylinders. *J. Fluid Mech.* **242**, 31–50.

FALTINSEN, O., & LØKEN, A. 1978 Drift forces and slowly-varying horizontal forces on a ship in waves. In *Proc. Symposium on Applied Mathematics dedicated to the late Prof. Dr. R. Timman, Delft University,* pp. 22–41.

FALTINSEN, O., NEWMAN, J. N. & VINJE, T. 1995 Nonlinear wave loads on a slender vertical cylinder. *J. Fluid Mech.* **289**, 179–199.

HAVELOCK, T. H. 1929 Forced surface-waves on water. *Phil. Mag.* (7) **8**, 569–576.

HAVELOCK, T. H. 1940 The pressure of water waves upon a fixed obstacle on water. *Proc. R. Soc. Lond.* A **175**, 409–421.

HUNT, J. N. & BADDOUR, R. E. 1981 The diffraction of nonlinear progressive waves by a vertical cylinder. *Q. J. Mech. Appl. Maths* **34**, 69–88.

HUNT, J. N. & WILLIAMS, A. N. 1982 Non linear diffraction of Stokes water waves by a circular cylinder for arbitrary uniform depth. *J. Méc. Théor. Appl.*, **1**, 429–449.

JOHN, F. 1950 On the motion of floating bodies, II. *Commun. Pure Appl. Maths* **3**, 45–101.

JONES, D. S. 1964 *The Theory of Electromagnetism.* Pergamon.

KIM, M.-H. & YUE, D. K. P. 1989 The complete second-order diffraction solution for an axisymmetric body. Part 1. Monochromatic incident waves. *J. Fluid Mech.* **200**, 235–264.

LIGHTHILL, M. J. 1979 Waves and hydrodynamic loading. In *Proc. 2nd Intl Conf on the Behaviour of Offshore Structures,* vol. 1, pp. 1–40. Cranfield: BHRA Fluid Engineering.

LINTON, C. M. & EVANS, D. V. 1990 The interaction of waves with arrays of vertical circular cylinders. *J. Fluid Mech.* **215**, 549–569.

MACCAMY, R. C. & FUCHS, R. A. 1954 Wave forces on a pile: a diffraction theory. *Tech. Memo.* 69, US Army Corps of Engineers.

MALENICA, Š. & MOLIN, B. 1995 Third-harmonic wave diffraction by a vertical cylinder. *J. Fluid Mech.* **302**, 203–229.

MCIVER, M. 1994 Second-order wave diffraction in two dimensions. *Appl. Ocean Res.* **16**, 19–25.

MEI, C. C. 1983 *The Applied Dynamics of Ocean Waves.* Wiley.

MOLIN, B. 1979 Second order diffraction loads upon three dimensional bodies. *Appl. Ocean Res.* **1**, 197–202.

MOLIN, B. 1994 Second-order hydrodynamics applied to moored structures – a state-of-the-art survey. *Schiffstechnik.* **41**, 2, 59–84.

NEWMAN, J. N. 1990 Second-harmonic wave diffraction at large depths. *J. Fluid Mech.* **213**, 59–70.